Behaviour of Dense Frederikshavn Sand During Cyclic Loading

Nielsen, Søren Kjær; Shajarati, Amir; Sørensen, Kris Wessel; Ibsen, Lars Bo

Publication date:
2012

Document Version
Accepted author manuscript, peer reviewed version

Behaviour of Dense Frederikshavn Sand During Cyclic Loading

Søren Kjær Nielsen
Amir Shajarati
Kris Wessel Sørensen
Lars Bo Ibsen

ISSN 1901-7278
DCE Technical Memorandum No. 15

AALBORG UNIVERSITY
Department of Civil Engineering

Aalborg University
Department of Civil Engineering
Geotechnical Engineering

DCE Technical Memorandum No. 15

Behaviour of Dense Frederikshavn Sand During Cyclic Loading

by

Søren Kjær Nielsen
Amir Shajarati
Kris Wessel Sørensen
Lars Bo Ibsen

June 2012

Scientific Publications at the Department of Civil Engineering

Technical Reports are published for timely dissemination of research results and scientific work carried out at the Department of Civil Engineering (DCE) at Aalborg University. This medium allows publication of more detailed explanations and results than typically allowed in scientific journals.

Technical Memoranda are produced to enable the preliminary dissemination of scientific work by the personnel of the DCE where such release is deemed to be appropriate. Documents of this kind may be incomplete or temporary versions of papers—or part of continuing work. This should be kept in mind when references are given to publications of this kind.

Contract Reports are produced to report scientific work carried out under contract. Publications of this kind contain confidential matter and are reserved for the sponsors and the DCE. Therefore, Contract Reports are generally not available for public circulation.

Lecture Notes contain material produced by the lecturers at the DCE for educational purposes. This may be scientific notes, lecture books, example problems or manuals for laboratory work, or computer programs developed at the DCE.

Theses are monograms or collections of papers published to report the scientific work carried out at the DCE to obtain a degree as either PhD or Doctor of Technology. The thesis is publicly available after the defence of the degree.

Latest News is published to enable rapid communication of information about scientific work carried out at the DCE. This includes the status of research projects, developments in the laboratories, information about collaborative work and recent research results.

Published 2012 by
Aalborg University
Department of Civil Engineering
Sohngaardsholmsvej 57,
DK-9000 Aalborg, Denmark

Printed in Aalborg at Aalborg University

ISSN 1901-7278
DCE Technical Memorandum No. 15

Behaviour of Dense Frederikshavn Sand During Cyclic Loading

Søren Kjær Nielsen[1] Amir Shajarati[1] Kris Wessel Sørensen[1] Lars Bo Ibsen[2]

Department of Civil Engineering, Aalborg University

Abstract

This article investigates how Frederikshavn Sand behaves when subjected to cyclic loading with emphasis on the development of deformations and the number of cycles, which it can withstand before failure is reached. The investigation is done by performing a series of undrained cyclic triaxial tests, at the Geotechnical Laboratory at Aalborg University. Tests were conducted with a relative density of 80 % in order to simulate offshore conditions where relative densities are relatively high. The purpose is to develop design diagrams, which can be used in order to estimate the undrained cyclic bearing capacity of Frederikshavn Sand for an arbitrary stress level and cyclic loading condition. It is discovered that the governing parameters regarding the response is dependent on the stress path and insitu conditions; initial pore pressure, stress state and the combination of average and cyclic shear stresses.

1 Introduction

The Fatigue Limit State is very often the limiting design condition for offshore wind turbine foundations, which is due to the fact that these foundations are subjected to severe cyclic loading through current, wave and wind actions. During the lifetime of an offshore wind turbine foundation, cyclic loading will correspond to a drained situation since excess pore pressure is able to dissipate between storms. However, during a single storm the drainage path may be long compared to the permeability of the soil, and cyclic loading from a storm may therefore lead to an undrained situation. The tests in this article should imitate cyclic loading during a storm, hence the tests are conducted undrained.

When designing an offshore wind turbine foundation no common design regulation exists regarding cyclic loading. Hence, different approaches have been made as an attempt to include cyclic loading in the design procedure. One method is by the application of design graphs, which accounts for the stresses generated by cyclic loads and the deformations they lead to. These graphs are based on laboratory work in the form of cyclic triaxial or cyclic direct simple shear tests.

The design graphs resulting from the cyclic triaxial tests are to be applied in connection with the construction of an offshore windturbine foundation in Frederikshavn, Denmark. The soil at this location is a marine sand defined as *Frederikshavn Sand*. This paper characterises the Frederikshavn Sand, which the cyclic triaxial tests have been conducted on, and the course of action regarding the execution of cyclic triaxial tests. Furthermore, it is described how Frederikshavn Sand reacts during undrained cyclic loading, which can be applied in a design diagram.

2 Characteristics of Cyclic Loading

Offshore cyclic loading is irregular, where both load period and amplitude changes over time. For laboratory work, however, the cyclic loads are simplified from irregular to regular with a constant period and amplitude. The cyclic load is defined by the cyclic shear stress, τ_{cy}, and the average shear stress, τ_a, with corresponding shear strain, γ_{cy} and γ_p, which is illustrated in Figure 1. τ_a consists of two parts: τ_0 which is the the shear stress obtained from the

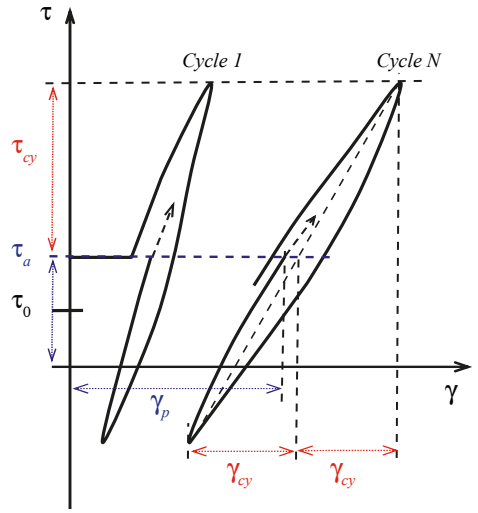

Figure 1: *Stress-strain behaviour under cyclic loading.*

[1] *M.Sc. Student, Department of Civil Engineering, Aalborg University, Denmark*

[2] *Prof., Department of Civil Engineering, Aalborg University, Denmark*

insitu condition, and $\Delta\tau_a = \tau_a - \tau_0$ which is the average shear stress from further loading. This can include the self-weight of a structure and the mean shear stress created by cyclic loading.

During a cyclic triaxial test the soil will experience the cyclic shear stress, τ_{cy}, about the average shear stress, τ_a, see Figure 2(a). The cyclic load depicted in Figure 2(a) gives rise to pore pressure build-up defined by a permanent pore pressure component, u_p, and a cyclic pore pressure component, u_{cy}, as seen in Figure 2(b). As the pore pressure components continue to increase over time it causes a decrease in effective stresses which results in larger and larger permanent shear strain, γ_p, and cyclic shear strains as well, γ_{cy}, see Figure 2(c) (Andersen, 2009). It should be noted, however, that the example given above is not always the case. There are situations where the pore pressure and shear strain evolution responds differently (Shajarati et al., 2012).

The undrained response of a sand is dependent on the relative density. A loose sand will try to compact, and positive pore pressure is generated, which reduces the effective stresses. A dense sand will try to dilate, which results in negative pore pressure. This entails that after initial undrained loading the effective stresses for a dense sand will be increased, and for a loose sand, it will decrease. This is decisive for how the initial stress path will look like. In Figure 3 an example of a loose sand is given. It is seen that the effective stresses decrease as cyclic loading continues, and the stress path will eventually intersect the failure envelope. For a dense sand the arc of the initial stress path will first go towards larger effective stresses, and thereafter the effective stresses will start to decrease as pore pressure builds up.

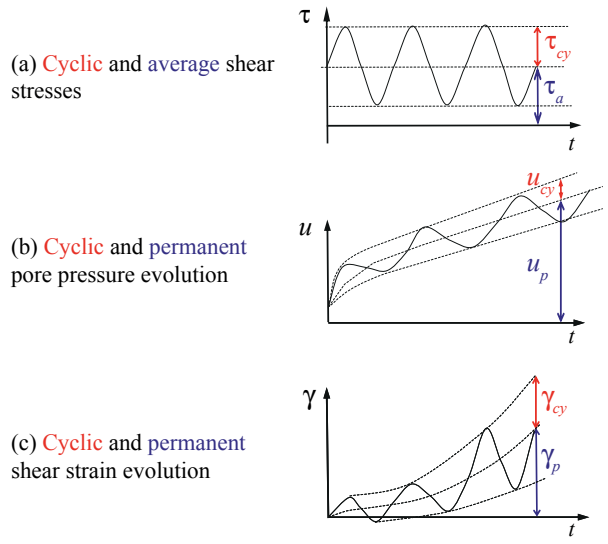

Figure 2: *Shear stress, pore pressure and shear strain as a function of time during undrained cyclic loading.*(Andersen, 2009)

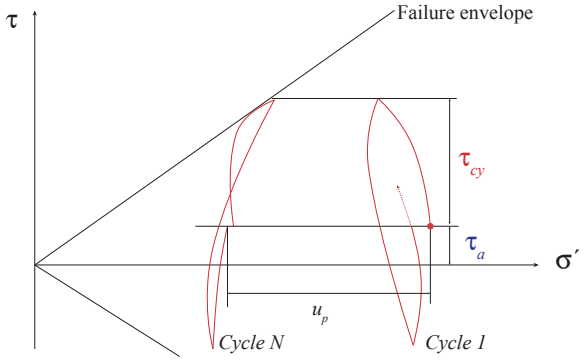

Figure 3: *Effective stress path for undrained cyclic triaxial test.*(Andersen, 2009)

3 Soil and Test Specifications

The Frederikshavn Sand has a minimum and maximum void ratio of $e_{min} = 0.64$ and $e_{max} = 1.05$. The preparation method for the triaxial sample was made by dry tamping to a relative density of $I_D = 80$ %, using undercompaction with 5 layers. When saturating the specimens, the stiffness of the soil skeleton, i.e. the bulk modulus, K, and the pore pressure level were taken into account (Amar, 1992). Through a consolidation test K was determined to be 108 MPa and it was insured that the samples were at least 99.9 % saturated.

Drained preshearing of 400 cycles with an amplitude of $0.04\,\sigma'_{vc}$ was applied, at an effective mean stress level of 30 kPa, in order to remove any stress concentration from tamping and thereby creating a more homogeneous sample. The effective mean stress was afterwards raised to 60 kPa.

Through an earlier study made on Frederikshavn Sand by Hansson et al. (2005) an expression for the friction angle as a function of relative density, I_D, and confining pressure, σ'_3, was calibrated to

$$\varphi = 0.146\ I_D + 41\ \sigma_3'^{-0.0714} - 1.78^\circ \qquad (1)$$

The expression has been validated by conducting three drained isotropic consolidated monotonic tests with an effective confining pressure in the range between 30 and 120 kPa. The deviation between the results and the expression is in the interval 1-5 %. From the monotonic tests the triaxial friction angle was found to be $\varphi = 39.6^\circ$ for an effective isotropic consolidation stress of 60 kPa. Thereby giving a K_0 value of 0.36. This produces an anisotropic consolidation with an effective vertical consolidation stress, σ'_{vc}, of 166.7 kPa and an effective horizontal consolidation stress, σ'_{hc} of 60 kPa.

The test samples were cylindrical with an initial height, H_0, of 71 mm, and an initial diameter, D_0, of 70 mm, hence H/D $\approx$ 1. At the cap and base, two rubber membranes with high vacuum grease in between were placed to make the cap and base frictionless. These initiatives were performed in order

Table 1: *Average and cyclic shear stress used in the test programme. Test No. 1 is a monotonic test, and test No. 2-17 is cyclic triaxial tests.*

Test No.	τ_a [kPa]	τ_{cy} [kPa]	u_0 [kPa]
1	400.2	0.0	110.7
2	209.8	185.2	105.8
3	260.2	100.8	109.2
4	166.9	167.2	110.0
5	129.6	99.9	100.0
6	124.9	49.8	110.1
7	78.0	50.2	120.7
8	53.4	17.0	100.2
9	166.6	167.1	302.3
10	49.6	125.5	99.8
11	24.0	50.9	139.7
12	24.6	100.2	100.3
13	24.8	100.5	160.6
14	24.8	100.4	299.7
15	66.0	125.6	99.5
16	84.1	129.4	100.4
17	158.8	216.9	100.4

to ensure homogeneous stress distribution throughout the sample (Ibsen and Lade, 1998a).

During sample preparation, which included installation, pre-shearing and consolidation, it was found that the height decreased with a maximum value of 1 %.

4 Cyclic Test Programme

A total of 17 undraind triaxial tests were conducted; 1 monotonic and 16 cyclic tests. 13 of the cyclic triaxial tests were performed with different combinations of average shear stress, τ_a, and cyclic shear stress, τ_{cy}. These tests are used for constructing the design graphs described in section 6. A complete list of the conducted tests are shown in Table 1

4.1 Cyclic Triaxial Cell

In Figure 4 a sketch of the cyclic triaxial cell is shown. The principle of the system is that a cyclic load is applied via the hydraulic piston at the bottom of the cell.

In order to calculate the stresses and strains in the sample, the following parameters were measured from the triaxial apparatus:

- Axial deformations
- Cell pressure
- Pore pressure
- Piston force

4.2 Test Procedure

As mentioned, the dominating force on offshore wind turbine foundations is wave loads, which have

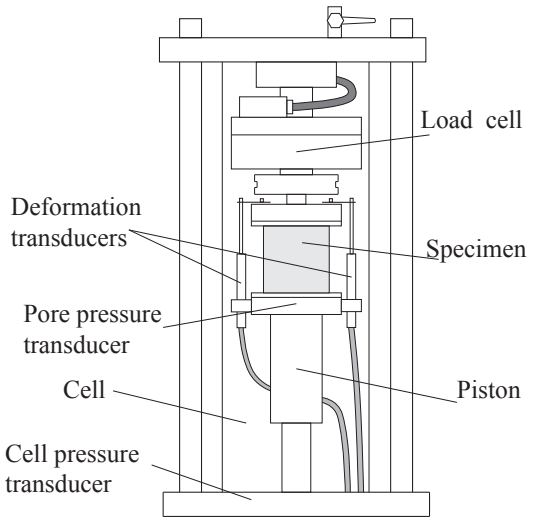

Figure 4: *Illustration of the cyclic triaxial cell.*

a period of 10 to 20 seconds (Lesny, 2010). According to Andersen (2009) the load period on sand seem to have no significant effect when a test is conducted undrained, and therefore the length of the period is only limited by the reaction time of the hydraulic piston. Based on this information the load period was kept as low as practically possible in the range from 10 to 100 seconds, to limit test duration.

To reflect the insitu conditions the sample was anisotropicly consolidated. The process of consolidating the sample and conducting cyclic tests is illustrated in Figure 5, and described in the following. **(a) isotropic consolidation 1**: The sample was set up in the triaxial cell where it was exposed to an isotropic stress level of 30 kPa. **(b) preshearing**: The sample was presheared in order to remove stress concentrations originating from tamping when using the undercompaction method. Preshearing was performed at lower isotropic stress levels, than when the K_0 procedure was applied in order not to consolidate the soil too much during preshearing. **(c) isotropic consolidation 2**: After preshearing the confining pressure was increased to an isotropic stress level of 60 kPa in order to have horizontal stresses corresponding to insitu conditions. **(d) Anisotropic consolidation**: This step is the actual K_0 procedure where the vertical stress was increased so it corresponds to insitu conditions ($\sigma'_{vc} = 166.7$ kPa, $\sigma'_{hc} = 60$ kPa). **(e) Cyclic loading**: The processes up till cyclic loading were conducted drained. From the K_0 point the increase in average shear stress, $\Delta\tau_a$, and the cyclic shear stress, τ_{cy}, was added undrained.

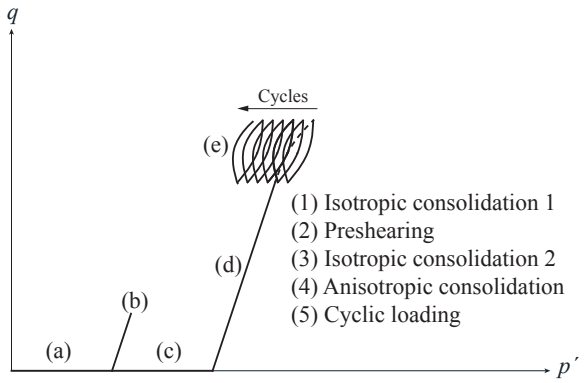

Figure 5: Illustration of test procedure during cyclic triaxial tests.

5 Cyclic Test Results

When analysing the cyclic test results it is observed that the failure modes can be separated into two main groups. One where cyclic shear strain, γ_{cy}, is dominating, and another where permanent shear strain, γ_p, is dominating. A common feature of the tests that fail with dominating γ_p is that they are all subjected to one-way loading, i.e. $\tau_a > \tau_{cy}$. The opposite effect is observed when γ_{cy} is dominating, i.e. $\tau_a < \tau_{cy}$. Another observation is that all one-way loaded tests fail by incremental collapse, while all two-way loaded tests fail by liquefaction. This will be outlined in the following sections.

For all the tests failure is defined as either $\gamma_p = 15$ % or $\gamma_{cy} = 15$ %. A plot of the different tests with number of cycles to failure can be seen in Figure 6.

5.1 Liquefaction

The stress path in the $p' - q$ space for a two-way loaded cyclic test with $\tau_a = 25$ kPa and $\tau_{cy} = 100$ kPa is depicted in Figure 7. The sample is subjected to cyclic loading with an amplitude so large, that the excess pore pressure, u, exceeds the effective mean stresses, p', which becomes zero, and thereby liquefaction occurs. The stress path has the characteristic butterfly shape as described in Randolph and Gouvernec (2011). At liquefaction the sample will start to dilate, which generates negative pore pressure, and effective stresses are again mobilised, and cyclic loading continues.

From Figure 8 it is observed that the initial pore pressure is equal to 300 kPa indicated by point (a), which means that the confining pressure is 360 kPa in order to keep effective mean stresses equal to 60 kPa. As the sample is exposed to more cycles the pore pressure will eventually increase to a value of 360 kPa, indicated by point (b), which is the point where liquefation occurs.

When liquefaction occurs the soil has lost its bearing capacity, which produces large shear deformations as seen in Figure 9. During all the cyclic tests

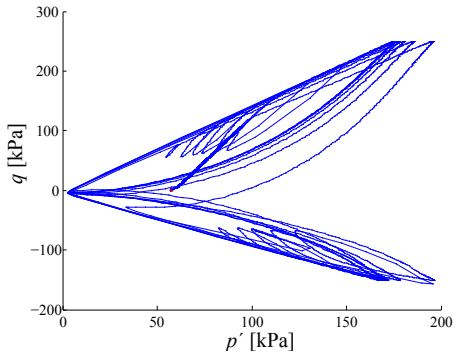

Figure 7: *$p' - q$ diagram for a cyclic triaxial test, where liquefaction is observed. The test failed at $N = 8$ with $\tau_a = 25$ kPa and $\tau_{cy} = 100$ kPa.*

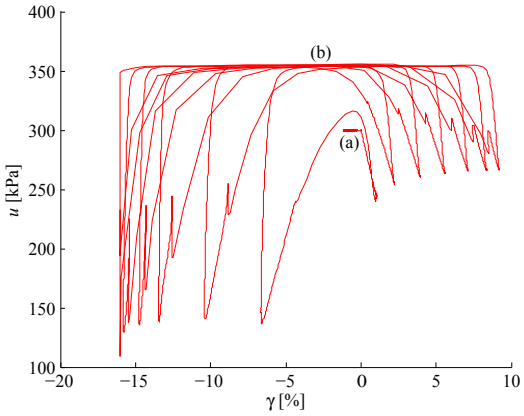

Figure 8: *Excess pore pressure development as a function of cyclic shear strains during cyclic triaxial test. The test failed at $N = 8$, with $\tau_a = 25$ kPa and $\tau_{cy} = 100$ kPa.*

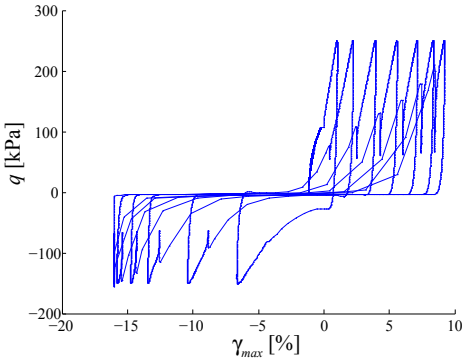

Figure 9: *γ - q diagram for a cyclic triaxial test, where liquefaction is observed. Large shear strains develops when q becomes zero. $N = 8$, $\tau_a = 25$ kPa and $\tau_{cy} = 100$ kPa.*

where liquefaction occurs, liquefaction is observed two times in each cycle; once in compression and once in extension. For each time liquefaction occurs, the shear strain increases as cyclic loading continues, as seen in Figure 9.

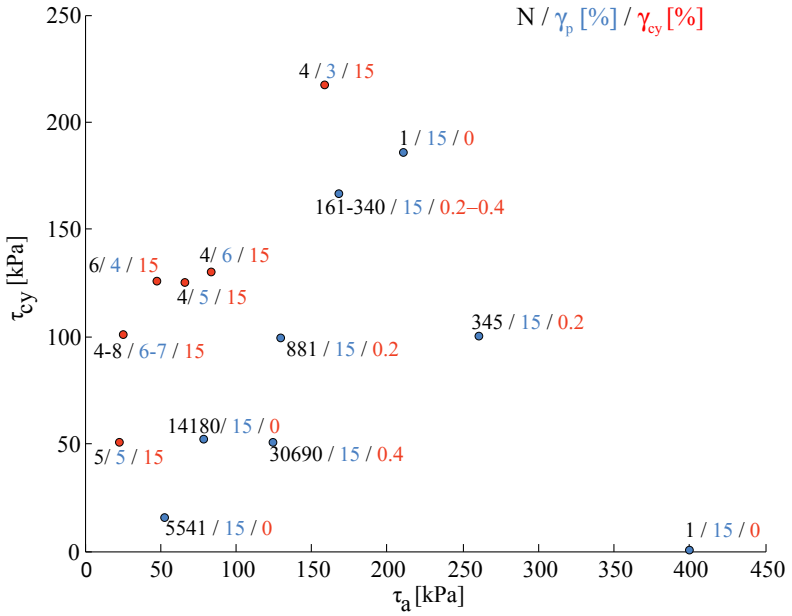

Figure 6: *Test results of the 13 different cyclic triaxial tests and 1 monotonic test.*

5.2 Incremental Collapse

Figure 10 shows a one-way loaded test with $\tau_a = 167$ kPa and $\tau_{cy} = 167$ kPa. The response shows that as cyclic loading is being applied p' decreases, which is due to pore pressure build up. The pore pressure development is illustrated in Figure 11, and it is observed that initially the pore pressure decreases because the sample tries to dilate resulting in an increase in effective mean stresses. As cyclic loading continues the pore pressure starts to increase entailing a reduction in effective mean stresses.

Moreover, from Figure 10 it is observed that the inclination of the cycles becomes steeper as more cycles are applied, which is due to an increase in soil stiffness. This means that γ_{cy} becomes smaller as N increases.

In Figure 12, which shows a γ - q diagram, it is observed that the incremental shear strain decreases, but the total shear strain increases with number of cycles. This type of failure is also defined as incremental collapse by Peralta (2010).

Figure 13 also confirms the statement that the incremental shear strain decreases with increasing number of cycles, while the permanent shear strain increases and eventually resulting in failure at $\gamma_p = 15$ % for $N = 340$ cycles.

6 Design Graphs

When constructing diagrams which can be applied in practical design situations, the average and cyclic shear stress are often normalised with respect to a

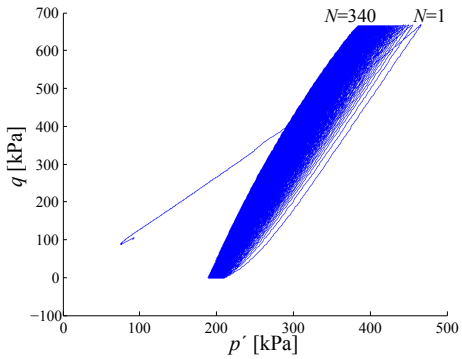

Figure 10: *Stress path in $p' - q$ space. The test is conducted with $\tau_a = 167$ kPa and $\tau_{cy} = 167$ kPa and failed at $N = 340$ cycles.*

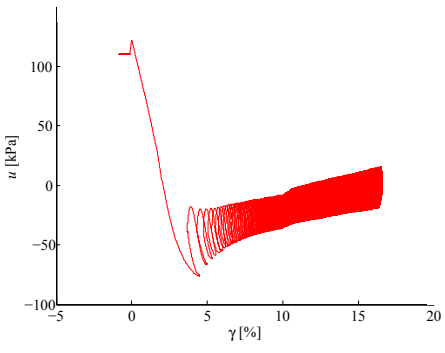

Figure 11: *Pore pressure development as a function of shear strains. The test is conducted with $\tau_a = 167$ kPa and $\tau_{cy} = 167$ kPa and failed at $N = 340$ cycles.*

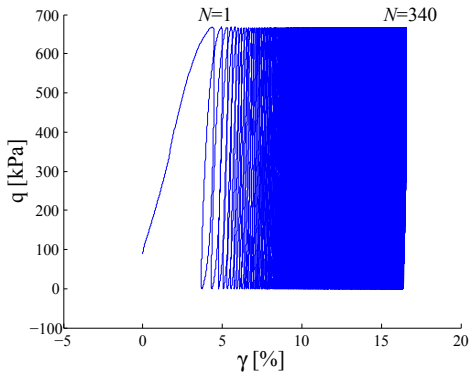

Figure 12: *$\gamma - q$ diagram for a test, which fails under incremental collapse. $N = 340$ cycles, $\tau_a = 167$ kPa and $\tau_{cy} = 167$ kPa.*

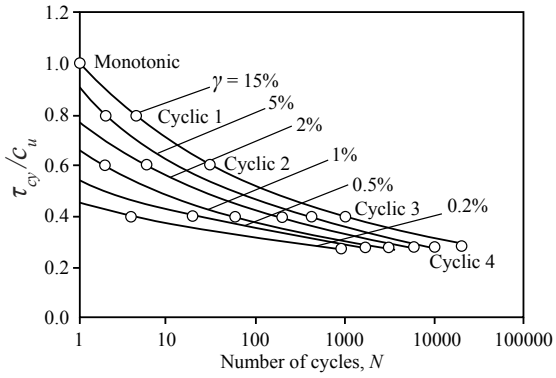

Figure 14: *Strain contour diagram for sand from cyclic simple shear tests with $\tau_a = 0$. (Randolph and Gouvernec, 2011)*

certain stress value. When this normalisation is performed the average and cyclic shear stresses are defined as *Average Load Ratio*, ALR, and *Cyclic Load Ratio*, CLR.

Different authors have proposed various types of design graphs for cyclic loading, which all take the cyclic shear stress into account via the cyclic load ratio. Randolph and Gouvernec (2011) made a *strain contour diagram*, shown in Figure 14, based on 1 undrained monotonic and 4 undrained cyclic simple shear tests on sand performed by Mao (2000). The diagram shows the strain contours as a function of the cyclic load ratio and number of cycles, and can thereby predict the shear strain from cyclic loading. However, during a literature study performed by Shajarati et al. (2012) and also by the conducted cyclic tests, it was found that both the cyclic and average shear stress level are very important, for the cyclic bearing capacity. Therefore strain contour diagrams, which only takes the cyclic load ratio into account, are insufficient for predicting the effects of cyclic loading.

Andersen and Berre (1999) made a study on the effects of cyclic loading, where both the cyclic load ratio and the average load ratio were taken into account. This produced the design graph in Figure 15, which was made for Baskarp sand with a relative density of 95 %. The normalisation in this diagram is performed with the effective vertical consolidation stress, σ'_{vc}, and it can be observed that failure is dependent on the combination of average and shear stresses. It should be noted that in this graph cyclic failure is defined as either 3% cyclic or permanent shear strain, and the tests were conducted with H/D = 2.

When cyclic soil testing is conducted on sand, the cyclic and average shear stress is most often normalised with respect to σ'_{vc}, as shown in Figure 15 (Andersen and Berre, 1999). This is useable under drained conditions since the drained failure envelope is only dependent on the friction angle and effective mean stress, and σ'_{vc} can therefore be used as a normalisation parameter.

In the undrained case however, the undrained shear strength for a dilative sand is not only dependent on the friction angle and mean effective stresses, but also the amount of initial pore pressure (Ibsen and Lade, 1998b). This is due to the fact that the undrained shear strength is influenced by cavitation. Before a dense sand reaches failure (both in tension and extension) it tries to dilate, which generates negative excess pore pressure and thereby an

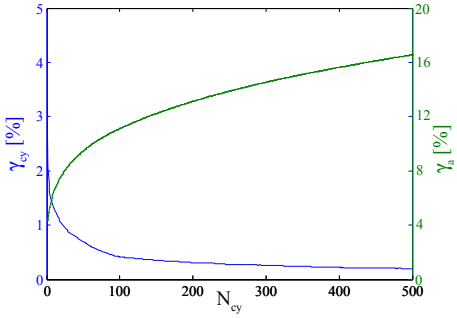

Figure 13: *Number of cycles - γ diagram. $N = 340$ cycles, $\tau_a = 167$ kPa and $\tau_{cy} = 167$ kPa.*

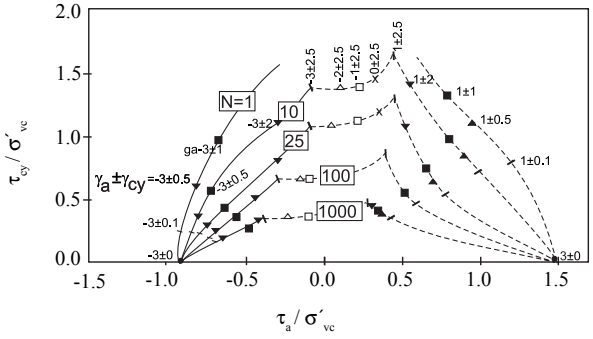

Figure 15: *Strain contour diagram for dense Baskarp sand in the undrained state. (Andersen and Berre, 1999)*

increase in effective stresses. At first this will "eat" the initial pore pressure and afterwards cavitation will occur at around u = -95 kPa, which will lead to failure. Even though this is a well known problem, the normalisation parameter for dense sand in the undrained state is still most often σ'_{vc}, as seen in Figure 15, which does not account for cavitation and the initial pore pressure.

6.1 Undrained Shear Strength

As mentioned σ'_{vc} can in the drained case be related to the drained shear strength, τ_f. The drained shear strength accounts for the friction angle, the effective mean stress and cohesion, and is given as

$$\tau_f = \frac{1}{2} \cdot \frac{6 \sin\varphi}{3 - \sin\varphi} \left(p' + c' \cot\varphi'\right) \qquad (2)$$

where $c' = 0$ for cohesionless soils. Instead of using σ'_{vc} as a normalisation parameter in the undrained case for sand, the undrained shear strength, c_u, is used. Therefore, the use of the above expression is extended to the undrained case by adding the initial pore pressure, u_0, and the pore pressure at which cavitation occurs u_{cav}, which results in equation (3). Furthermore, the used effective mean stress corresponds to failure in the drained case, p'_{df}.

$$c_u = \frac{1}{2} \cdot \frac{6 \sin\varphi}{3 - \sin\varphi} \left(p'_{df} + u_0 + u_{cav}\right) \qquad (3)$$

The argument for using the above expression is that the undrained bearing capacity for a dense sand is governed by cavitation, as negative pore pressure develops during loading (Ibsen and Lade, 1998b). It is therefore important to include the pore pressure when calculating c_u in the undrained case for sand. The effect of adding the initial pore pressure, u_0, and the pore pressure at cavitation, u_{cav}, is illustrated in Figure 16. The figure illustrates the effective stress paths for two examples with the same initial effective mean stress, p'_0. The two examples end up having a different undrained shear strength, because of differences in initial pore pressure. Following the total stress path will lead to drained failure in point (a), which is the point where p'_{df} is measured. From this point the amount of initial pore pressure and the pore pressure at cavitation is added to p'_{df}. This means that a higher amount of initial pore pressure will lead to a higher value of the undrained shear strength before failure is reached, which is illustrated by point (b) and (c).

6.2 Modified Design Graph

Based on the expression for undrained shear strength in equation (3), a *modified design diagram* is constructed for the Frederikshavn Sand in the undrained case with I_D = 80 %. The modified design diagram is based on the 17 conducted tests and normalised with respect to c_u, as shown in Figure 17. It is seen that the graph shares the same tendency as the design graph by Andersen and Berre (1999) in Figure 15. However, an important feature of the modified design graph is that it accounts for the initial pore pressure, which is important when dealing with the undrained bearing capacity.

To illustrate the limitations of the design graph when normalising with σ'_{vc} as proposed by Andersen and Berre (1999), a comparison between the two design graphs can be seen in Figure 18. To make the comparison, three cyclic tests were conducted with the same average shear stress, τ_a = 25 kPa, and same cyclic shear stress, τ_{cy} = 100 kPa, but with different values of initial pore pressure, u_0, namely 100, 160 and 300 kPa. The calculated cyclic and average load ratios for the two design graphs can be seen in Table 2.

Table 2: *Three cyclic tests with τ_a = 25 kPa, τ_{cyc} =100 kPa and different initial pore pressure, u_0.*

	Design Graph		Modified Design Graph	
u_0	τ_a/σ'_{vc}	τ_{cy}/σ'_{vc}	τ_a/c_u	τ_{cy}/c_u
100 kPa	0.15	0.6	0.07	0.29
160 kPa	0.15	0.6	0.06	0.26
300 kPa	0.15	0.6	0.05	0.20

Figure 18(a) plots the three tests in the same point since they have the same ALR and CLR when normalising with σ'_{vc}. However, Figure 18(b) normalises with c_u and plots the three tests in different positions, because ALR and CLR is dependent on the initial pore pressure. The example given above illustrates that it is very important to construct a design diagram in a manner which represent the insitu conditions as good as possible. Therefore, if the drained state is the design case it is sufficient to apply σ'_{vc} as a normalisation parameter. On the other hand if the undrained state is the design case, the initial pore pressure should be taken into consideration, and therefore c_u should be used when normalising the design diagram.

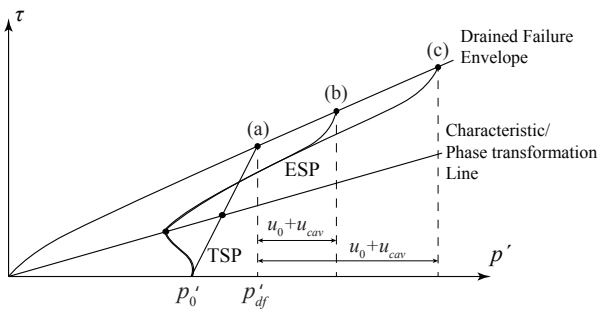

Figure 16: *Illustration of the theoretically effect of including initial pore pressure and the pore pressure at cavitation to the drained failure criterion.*

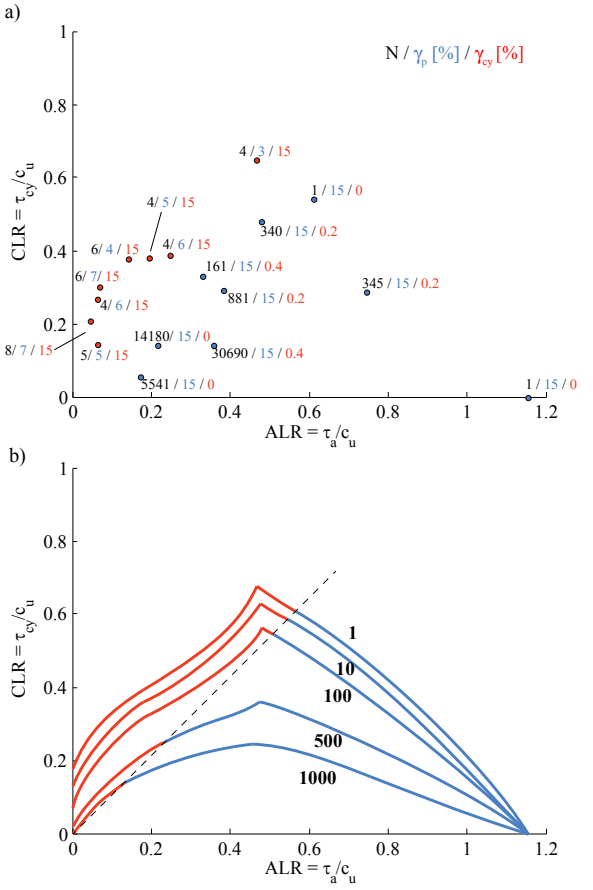

Figure 17: *Modified design diagram for Frederikshavn Sand in the undrained case with $I_D = 80$ %. Red corresponds to two-way loading, while blue is one-way loading.*

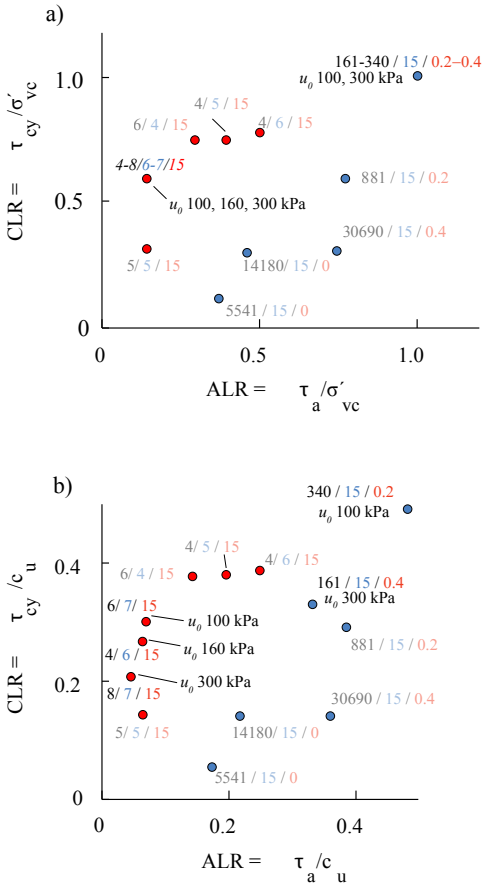

Figure 18: *Comparison between design graphs. (a) Normal design graph (σ'_{vc}). (b) Modified design graph (c_u)*

7 Conclusion

A modified design diagram is created for the Frederikshavn Sand in the undrained case for a relative density of $I_D = 80$ %. It can be used to estimate the number of cycles to failure for a given combination of pore pressure, average and cyclic load ratio.

When normalising cyclic and average shear stresses for use in design diagrams σ'_{vc} is found insufficient to use as a normalisation parameter in the undrained case, as it does not take pore pressure into account. This is important, since the undrained shear strength for a dense sand is governed by cavitation. Therefore the undrained shear strength, c_u, is used as a normalisation parameter for the modified design graph and should be used for other design graphs in the undrained case.

When comparing Figure 15 and Figure 17 a considerable difference is observed at ALR = 0. The difference can be explained by a large difference in applied back pressure. In the tests performed by Andersen and Berre (1999) a backpressure in the range from 500 - 1800 kPa was applied. Compared to the tests conducted to make Figure 17 with a backpressure at around 100 kPa, the limit in τ_{cy} without reaching cavitation is raised significantly. This makes it possible to perform tests with a load ratio combination of $\tau_a/\sigma'_{vc} = 0$ and $\tau_{cy}/\sigma'_{vc} = 1.5$. If the same test is performed with a low back pressure, cavitation will occur, and the test will correspond to a monotonic test. This observation strengthens the argument, for choosing c_u as the normalisation parameter for the undrained case.

References

Amar, **1992**. Samuel Amar. *Triaxial testing.* Divisions de Mecanique des sols et Foundations, (Re.document no. ETC5-N 91.12), 1992.

Andersen, **2009**. Knut H. Andersen. *Bearing capacity under cyclic loading - offshore, along the coast, and on land. The 21st Bjerrum Lecture presented in Oslo, 23 November 2007.* Canadian Geotechnical Journal, 46(5), pp. 513–535, 2009.

Andersen and Berre, **1999**. Knut H. Andersen and Torlav Berre. *Behaviour of a dense sand under monotonic and cyclic loading.* ECSMGE XII Geotechnical Engineering for Transportation Infrastructure. Proc.,, 2, pages 667–676, 1999.

Hansson, Hjort, and Thaarup, **2005**. Martin Hansson, Troels H. Hjort, and Martin Thaarup. *Static and transient loading of the bucket foundation for offshore wind-turbines.* M.Sc. Thesis, Aalborg University, 2005.

Ibsen and Lade, **1998a**. Lars Bo Ibsen and Poul Lade. *The Role of the Characteristic Line in Static Soil Behavior.* Localization and Bifurcation Theory for Soils and Rocks, pages 221–230, 1998.

Ibsen and Lade, **1998b**. L.B. Ibsen and P.V. Lade. *The Strength and Deformation Characteristics of Sand Beneath Vertical Breakwaters Subjected to Wave Loading.* AAU Geotechnical Engineering Papers, (Soil Mechanics Paper No. 23), 1998.

Lesny, **2010**. Kerstin Lesny. *Foundations for Offshore Wind Turbines.* ISBN: 978-3-86797-042-6, 1. Edition. VGE Verlag GmbH, 2010.

Mao, **2000**. X. Mao. *The Behaviour of Three Calcareous Soils in Monotonic and Cyclic Loading.* Ph.D. Thesis, University of Western Australia, 2000.

Peralta, **2010**. Proserpine K. Peralta. *Dissertation: Investigations on the Behavior of Large Diameter Piles under Long-Term Lateral Cyclic Loading in Cohesionless Soil*, 2010.

Randolph and Gouvernec, **2011**. M. Randolph and S. Gouvernec. *Offshore Geotechnical Enigineering.* ISBN13: 978-0-415-47744-4, 1. Edition. Spon Press, 2011.

Shajarati, Sørensen, Nielsen, and Ibsen, **2012**. Amir Shajarati, Kris W. Sørensen, Søren K Nielsen, and Lars Bo. Ibsen. *Manual for Cyclic Triaxial Test.* ISSN: 1901-7278, DCE Technical Memorandum No. 14. Aalborg University, 2012.